ACS APPLIED MATERIALS & INTERFACES

Research Article

www.acsami.org

Electrochemically Synthesized Sb/Sb_2O_3 Composites as High-Capacity Anode Materials Utilizing a Reversible Conversion Reaction for Na-Ion Batteries

Kyung-Sik Hong, Do-Hwan Nam,* Sung-Jin Lim, DongRak Sohn, Tae-Hee Kim, and HyukSang Kwon*

Department of Materials Science and Engineering, Korea Advanced Institute of Science and Technology, 291 Daehak-ro, Yuseong-gu, Daejeon, Republic of Korea

Supporting Information

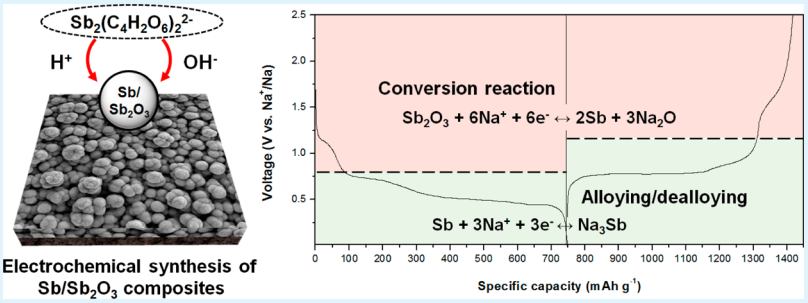

ABSTRACT: Sb/Sb_2O_3 composites are synthesized by a one-step electrodeposition process from an aqueous electrolytic bath containing a potassium antimony tartrate complex. The synthesis process involves the electrodeposition of Sb simultaneously with the chemical deposition of Sb_2O_3, which allows for the direct deposition of morula-like Sb/Sb_2O_3 particles on the current collector without using a binder. Structural characterization confirms that the Sb/Sb_2O_3 composites are composed of approximately 90 mol % metallic Sb and 10 mol % crystalline Sb_2O_3. The composite exhibits a high reversible capacity (670 mAh g^{-1}) that is higher than the theoretical capacity of Sb (660 mAh g^{-1}). The high reversible capacity results from the conversion reaction between Na_2O and Sb_2O_3 that occurs additionally to the alloying/dealloying reaction of Sb with Na. Moreover, the Sb/Sb_2O_3 composite shows excellent cycle performance with 91.8% capacity retention over 100 cycles, and a superior rate capability of 212 mAh g^{-1} at a high current density of 3300 mA g^{-1}. The outstanding cycle performance is attributed to an amorphous Na_2O phase generated by the conversion reaction, which inhibits agglomeration of Sb particles and acts as an effective buffer against volume change of Sb during cycling.

KEYWORDS: *antimony, antimony trioxide, electrodeposition, conversion reaction, anode, Na-ion battery*

1. INTRODUCTION

Recently, as the application of Li-ion batteries has extended to electric vehicles (EVs) and energy storage systems (ESSs), concerns about a continuous supply of Li and increasing Li prices have emerged. Na-ion batteries have attracted great attention as alternatives to Li-ion batteries, particularly for large-scale applications, due to low-cost and widespread Na resources.[1−3] For the practical use of Na-ion batteries, it is essential to develop efficient electrode materials with high specific capacity, long cycle life, and high rate performance.

Because Na and Li have similar chemical properties, alloying metals, which have been investigated for use in Li-ion batteries, have been pursued as possible anode materials for Na-ion batteries.[4−10] Among the candidates, Sb has been considered one of the most promising anode materials because of its high theoretical capacity (660 mAh g^{-1}) and relatively good kinetic properties. Nevertheless, a pure Sb electrode exhibits poor cyclability because it undergoes serious volume change (up to approximately 290%) during alloying/dealloying with Na, which leads to pulverization of the active material and electrical isolation from the current collector and consequently diminishes cycle stability. To alleviate the problems of volume change, Sb-M binary alloys (M = Al, Cu, Fe, Mo, etc.) and Sb-carbon composites have been investigated.[5,6,11−16] Darwiche et al.[12] reported an improvement in the electrochemical performance of Sb by alloying with Fe, where $FeSb_2$ exhibited excellent electrochemical performance, sustaining a reversible capacity exceeding 540 and 440 mAh g^{-1} over 130 cycles at currents of 36 and 300 mA g^{-1}, respectively. The improvement was attributed to the formation of a Na_3Sb/metallic Fe nanosized structure upon the first sodiation reaction of $FeSb_2$. In addition, electrospun Sb/C fibers have demonstrated enhanced cycling stability with 75% capacity retention after 300 cycles due to the buffer effects of a carbon matrix.[5] Although notable improvements have been achieved by the composites of Sb and metals or carbonaceous materials, the reduction in specific capacity

Received: May 15, 2015
Accepted: July 17, 2015
Published: July 17, 2015

DOI: 10.1021/acsami.5b04225
ACS Appl. Mater. Interfaces 2015, 7, 17264−17271

based on the total weight of an electrode cannot be avoided due to the high proportion of inactive materials in such composites.

Another effective approach to improve the cycle stability of Sb-based electrodes is to use a Na_2X (X = O, S, etc.) buffer matrix to relieve the stress generated by volume changes during cycling.[17,18] In the case of Sb_aX_b electrodes, during the discharge reaction, Sb_aX_b was converted into nanosized Sb crystallites dispersed in an amorphous Na_2X matrix. Because the Na_2X matrix is more ductile and softer than a metallic phase, the mechanical stress arising from the volume expansion of Sb particles can be effectively alleviated. Moreover, nanosized Sb crystallites produced by the conversion reaction have an advantageous effect on relieving the sodiation-induced stress. This is because the volumetric mismatch between unreacted and reacted parts of the particle would be reduced as the particle size decreases. Therefore, the structural stress caused by the volumetric mismatch during the cycling can be minimized by reducing the particle size.

In addition to this, antimony oxides (Sb_2O_3, Sb_2O_4, etc.) exhibit higher capacity than do pure Sb electrodes[19−21] because they can store Na ions via a conversion reaction and a further alloying reaction, as indicated by eq 1 and 2.

$$Sb_xO_y + 2yNa^+ + 2ye^- \leftrightarrow yNa_2O + xSb \quad (1)$$

$$yNa_2O + xSb + 3xNa^+ + 3xe^- \leftrightarrow yNa_2O + xNa_3Sb \quad (2)$$

A recent investigation on Sb_2O_4 electrodes showed that a large reversible capacity of 896 mAh g^{-1} at a C-rate of 1/70 could be made while retaining a reversible capacity of 724 mAh g^{-1} after 20 cycles.[19] This result suggests that more Na ions and electrons (~8 mol of Na^+ and e^-) can be stored through the conversion reaction of Sb_2O_4. Moreover, Hu et al. demonstrated that Sb_2O_3 undergoes combined conversion-alloying electrochemical reactions in Sb_2O_3 with a high specific capacity of 509 mAh g^{-1}.[20] It is worthwhile to note that antimony oxides deliver much higher specific capacities compared with the Sb-M binary alloys and Sb-carbon composites because antimony oxides have no capacity reduction by the inactive component. Despite their high theoretical capacity, however, antimony oxide anode materials are limited in practical utilization because conversion reactions usually suffer from large voltage hysteresis, low reversibility, and high redox potential.[22]

In this study, therefore, Sb/Sb_2O_3 composites composed of mainly metallic Sb and small amounts of Sb_2O_3 was synthesized by electrodeposition to achieve both an increase in an available specific capacity and an improvement in cycle stability. The electrodeposition process allows facile control over the composition ratio of Sb and Sb_2O_3 by adjusting the applied current and bath composition.[23] Moreover, the synthesis of electrodes by an electrodeposition process is a one-step process without mixing with conductive agent and binder whereas the fabrication of an electrode by the conventional slurry coating process needs multiple-step processes involving slurry mixing, coating, and drying. The research objective of the present work is first to fabricate the Sb/Sb_2O_3 composites with the optimal composition of Sb and Sb_2O_3 by electrodeposition, and second to elucidate the sodiation/desodiation mechanism of the electrochemically synthesized Sb/Sb_2O_3 composites, and last to evaluate the feasibility of the composite as a high performance anode material for Na-ion batteries.

2. EXPERIMENTAL SECTION

An Sb/Sb_2O_3 composite electrode was prepared by galvanostatic electrodeposition from an electrolytic bath containing 0.025 M $K_2Sb_2(C_4H_2O_6)_2{\cdot}3H_2O$ (Sigma-Aldrich), 0.1 M KCl (Junsei), and 0.2 M $NaNO_3$ (Junsei). The electrodeposition of Sb/Sb_2O_3 composite was conducted at −4 mA cm^{-2} for 480 s, using a standard three-electrode cell; a nodule-type Cu foil was used as a working electrode, a pure Pt sheet as a counter electrode, and a saturated calomel electrode (SCE, 0.241 V vs SHE) as a reference electrode. The solution was stirred magnetically at ~240 rpm and maintained at room temperature throughout the electrodeposition. The Sb/Sb_2O_3 electrodeposits were dried in vacuum for 6 h after rinsing with distilled water to prevent oxidation. The weight of the Sb/Sb_2O_3 electrodeposits was estimated by subtracting the original weight of the nodule-type Cu foil from the total weight of the deposited film. The weight of the Sb/Sb_2O_3 electrodeposits was approximately 0.86 mg cm^{-2} (thickness of 1.34 μm).

The surface morphologies of the nodule-type Cu foil used as a substrate and the Sb/Sb_2O_3 composites were observed using scanning electron microscope (SEM). The crystal structures and chemical composition of the Sb/Sb_2O_3 composite were characterized by X-ray diffraction (XRD) and energy dispersive X-ray spectroscopy (EDS). Oxidation state analysis of Sb was conducted by X-ray photoelectron spectroscopy (XPS) on the surface of the Sb/Sb_2O_3 composite before and after ion etching for 60, 120, 180, and 240 s.

The electrochemical performance of the Sb/Sb_2O_3 composite was investigated using a two-electrode Swagelok-type cell with an electrode area of 1 cm^2 assembled in an Ar-filled glovebox.[24] The cell consisted of the Sb/Sb_2O_3 electrode as a cathode, pure Na (Sigma-Aldrich) as an anode, and 1 M $NaClO_4$ (Sigma-Aldrich) dissolved in anhydrous propylene carbonate (PC, Panax Etec) with 0.5 vol % of fluoroethylene carbonate (FEC, Panax Etec) as an electrolyte. An electrochemical test was conducted at a constant current of 66 mA g^{-1} over the potential range of 0.01−2.50 V vs Na^+/Na at 25 °C. For rate capability testing, the charge and discharge currents were varied from 66 to 3300 mA g^{-1} and returned to 66 mA g^{-1}. All electrodes were passed through a preformation cycle for stabilization. The phase transition of the composite during the sodiation/desodiation reaction was analyzed by *ex situ* XRD. For the *ex situ* XRD analysis, cycled electrodes were rinsed in anhydrous dimethyl carbonate (DMC, Panax Etec), and then the electrodes were sealed with Kapton tape in an Ar-filled glovebox to prevent them from being exposed to moisture. The bond between Sb and O of the composite was analyzed via Raman spectroscopy using a 785 nm laser as the excitation source over the range of 150−500 cm^{-1}.

3. RESULTS AND DISCUSSION

During the electrodeposition process of Sb from a potassium antimony tartrate electrolytic bath, the composition ratio of Sb and Sb_2O_3 varies with the reaction pathway associated with the local pH near the electrode.[23] In a strongly acidic environment, an antimony tartrate complex reduces to metallic Sb and the fully deprotonated form of tartaric acid on the electrode (reaction 3), that latter of which is then protonated into tartaric acid with H^+ in the electrolyte (reaction 4). It should be noted that this protonation reaction affects the local pH near the electrode. If the electrolyte is sufficiently acidic, the local pH is not greatly affected by the protonation reaction; however, when the concentration of protons in the electrolyte is not sufficient to compensate for the proton consumption of the protonation reaction in the vicinity of the electrode, the protonation reaction occurs through water decomposition (reaction 5) rather than proton consumption. The water decomposition reaction increases the local pH, and thus, the chemical deposition of Sb_2O_3 (reaction 6) occurs simultaneously with the electrodeposition of Sb (reaction 3). The composition ratio of Sb and Sb_2O_3 highly depends on the local pH in the vicinity

DOI: 10.1021/acsami.5b04225
ACS Appl. Mater. Interfaces 2015, 7, 17264−17271

of the electrode, and therefore the Sb/Sb_2O_3 composites with an optimal composition ratio can be fabricated by a simple modification of parameters such as the applied current density, the buffer capacity of the solution, and the electrolyte pH.

$$Sb_2(C_4H_2O_6)_2^{2-} + 6e^- \rightarrow 2Sb + 2(C_4H_2O_6)^{4-} \quad (3)$$

$$2(C_4H_2O_6)^{4-} + 4H^+ \rightarrow 2(C_4H_4O_6)^{2-} \quad (4)$$

$$2(C_4H_2O_6)^{4-} + 4H_2O \rightarrow 2(C_4H_4O_6)^{2-} + 4OH^- \quad (5)$$

$$Sb_2(C_4H_2O_6)_2^{2-} + 2OH^- + H_2O \rightarrow Sb_2O_3 + 2(C_4H_4O_6)^{2-} \quad (6)$$

Figure 1 shows the surface morphology of the nodule-type Cu foil and the electrodeposits. As described in the Experimental Section, we used a nodule-type Cu foil as a substrate to improve the adhesion between the electrodeposits and substrate by exploiting the mechanical interlocking effect of the nodules.[25] As shown in Figure 1a, the nodule-type Cu foil exhibited a rougher surface compared to that of conventional smooth Cu foil and consisted of spherical grains measuring approximately 1 μm. The electrodeposits show micrometer-sized morula-like particles uniformly deposited over the entire Cu substrate (Figure 1b). High-magnitude SEM image revealed that each morula-like particle was composed of agglomerated globular granules with interparticle voids (Figure 1b inset).

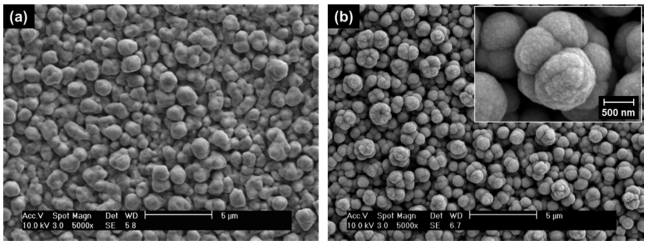

Figure 1. SEM images of (a) a nodule-type Cu foil and (b) Sb/Sb_2O_3 composites prepared by galvanostatic electrodeposition at −4 mA cm^{-2} for 480 s from an electrolytic bath containing 0.025 M $K_2Sb_2(C_4H_2O_6)_2{\cdot}3H_2O$, 0.1 M KCl, and 0.2 M $NaNO_3$ (Magnified image, inset).

EDS and XRD analyses were carried out to investigate the chemical composition and crystal structure of the electrodeposits. As shown in Figure 2a, EDS analysis confirms that the electrodeposits were only composed of Sb and O without any contaminations (the elemental contents of Sb and O were 96.49 wt % and 3.51 wt %, respectively). Figure 2b shows that the diffraction peaks for the electrodeposits were indexed to rhombohedral Sb (JCPDS Card no.85−1323) and cubic Sb_2O_3 (JCPDS Card no.71−0365), indicating that the electrodeposits consisted of crystalline Sb and crystalline Sb_2O_3. One distinguishing feature observed in the XRD pattern is that the crystallinity of Sb_2O_3 clearly increased compared to that of the Sb/Sb_2O_3 electrodeposits previously reported.[23] This result indicates that the crystal structure of Sb/Sb_2O_3 observed in this study became different from that previously reported[23] by modifying the deposition condition which could affect the nucleation and growth behavior of the electrodeposits.

To determine the distribution of Sb_2O_3 in the composite, the oxidation state of Sb in the electrodeposits was analyzed by XPS analysis before and after ion etching. As shown in Figure 3a, the XPS survey spectrum confirms the presence of Sb and O

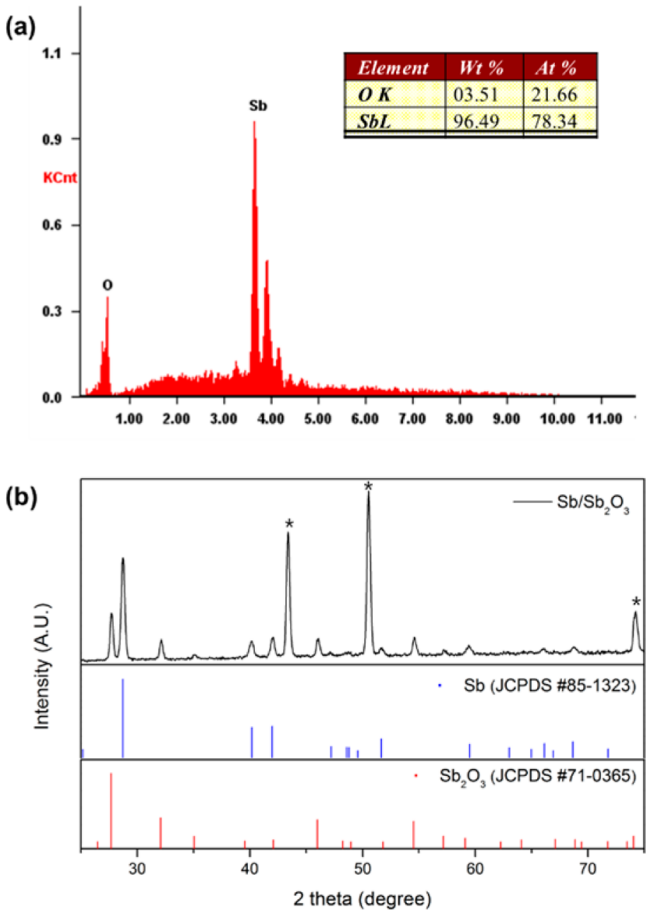

Figure 2. (a) EDS spectrum and (b) XRD pattern of Sb/Sb_2O_3 composites. (* denotes Cu substrate peak).

in accord with the EDS results (Figure 2a). A weak C 1s peak was attributed to adventitious carbon contamination. The Sb 3d spectrum exhibits two well-resolved signals before and after ion etching, corresponding to Sb $3d_{3/2}$ and Sb $3d_{5/2}$, due to the spin orbit coupling of the 3d state (Figure 3b). Before ion etching, the Sb $3d_{3/2}$ region shows two peaks at binding energies of 539.8 and 537.5 eV, corresponding to the Sb(III) and Sb(0) states, respectively. The Sb $3d_{5/2}$ spectrum shows overlapping O 1s and Sb(III) peaks at 530.4 eV and an Sb(0) peak at 528.2 eV, in good agreement with the results previously reported.[26,27] It is evident that large amounts of Sb_2O_3 and metallic Sb coexisted on the surface of the electrodeposits. After ion etching, all peaks related to the Sb(III) and Sb(0) states were clearly observed at all ion etching levels, whereas the intensity of the Sb(III) peaks decreased. The decrease in the intensity of the Sb(III) peaks after ion etching was due to the elimination of the surface oxide layer; similar results were obtained for pure Sb electrodeposits (data not shown). In addition, the area ratio of the Sb(III) peaks to the Sb(0) peaks remained nearly unchanged after ion etching for 60 s, which demonstrates that Sb_2O_3 was uniformly distributed over the inside of the electrodeposits but not on the surface oxide layer.

In this study, the composition ratio of Sb and Sb_2O_3 in the composite was estimated using EDS analysis and electrochemical measurement. Based on the EDS results shown in Figure 2a, assuming all of the detected oxygen is attributed to the Sb_2O_3 phase, the mole fraction of Sb_2O_3 in the composite was determined to be 10.2 mol %. Another way to estimate the

DOI: 10.1021/acsami.5b04225
ACS Appl. Mater. Interfaces 2015, 7, 17264−17271

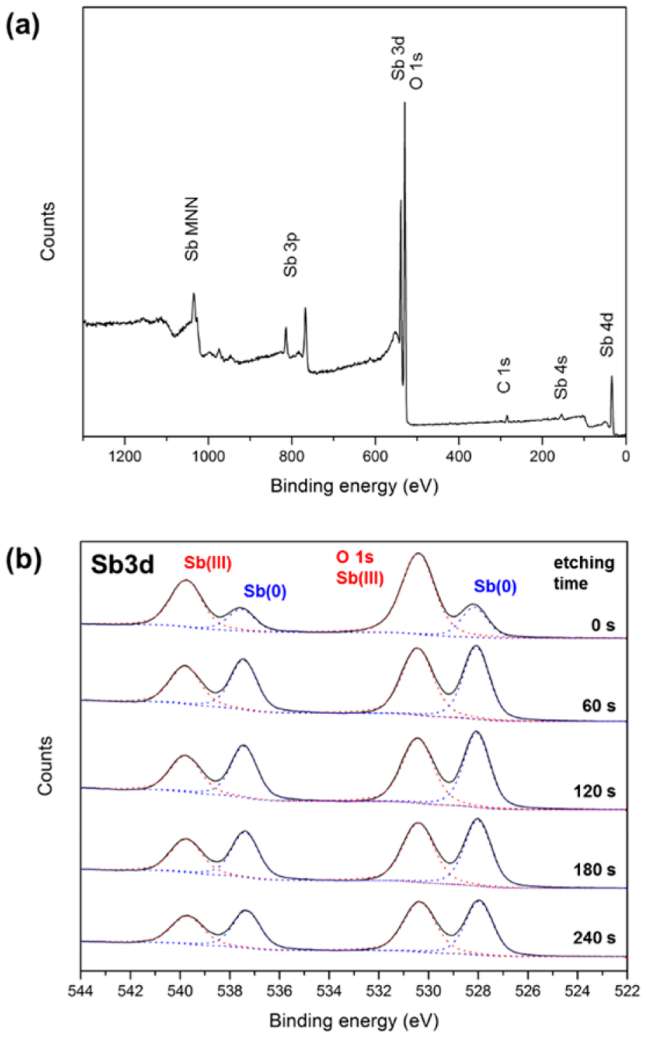

Figure 3. (a) An XPS survey Sb/Sb2O3 composites before and after etching for 60, 120, 180, and 240 s (top to bottom).

mole fraction of the electrodeposits is through an electrochemical approach. According to Faraday's law, the amount of metal reduced from metal ions is proportional to the quantity of charge passed; hence, the mole fraction of Sb could be estimated based on the total electric charge measured during electrodeposition. As mentioned earlier in this section, the electrochemical reaction and chemical reaction of the antimony tartrate complex occur simultaneously for the codeposition of Sb and Sb_2O_3. During the electrodeposition of Sb, three moles of electrons are required to obtain one gram equivalent of Sb (reaction 3). On the other hand, chemical deposition of Sb_2O_3 does not consume any electrons (reaction 6). In this respect, the weight difference between the calculated value based on Faraday's law and the actual measurement can be interpreted as the weight of Sb_2O_3. In this study, the measured weight of the electrode was 0.86 mg and the estimated weight of Sb was 0.71 mg (a current efficiency of 88.75%); thus, the weight difference was calculated to be 0.15 mg. In other words, the mole ratio of $Sb:Sb_2O_3$ was estimated to be 91.9:8.1 through the electrochemical approach. This result agrees well with the Sb_2O_3 mole fraction of 10 mol % measured by EDS analysis.

On the other hand, this mole ratio of $Sb:Sb_2O_3$ was not in accordance with the result of XRD or XPS analysis. Commonly, the mole ratio is relative to the intensity ratio of XRD peaks, but the peak intensity ratio cannot be directly converted into the mole ratio. To determine the exact mole ratio of each phase from a XRD pattern, a relation equation between the intensity ratio and composition ratio must be considered. Based on a relation equation for a Sb and Sb_2O_3 mixed system,[28] the molar percentage of Sb_2O_3 in the Sb/Sb_2O_3 composite was calculated to be approximately 5.7 mol %. However, this estimation could be inaccurate because the electrochemically synthesized Sb_2O_3 in the Sb/Sb_2O_3 composites had relatively low crystallinity.[23] If a substantial amount of amorphous Sb_2O_3 is excluded from the estimation of the composition using XRD analysis, the calculated mole fraction of Sb_2O_3 would be less than the actual amount of Sb_2O_3. On the contrary, the amount of Sb_2O_3 was overmeasured by XPS analysis due to the effects of preferential sputtering phenomenon.[29] In the case of metal and metal oxide mixed systems, the metal content of the surface become depleted during ion sputtering because metal oxides are more stable than metal to withstand ion bombardment without decomposition.[29] For the same reason, Sb_2O_3 was expected to be easily enriched at the surface of the composite after Ar^+ ion sputtering, and hence the amount of Sb_2O_3 would be overmeasured than the actual amount of Sb_2O_3. In this regard, the estimation of the composition ratio of Sb and Sb_2O_3 based on the electrochemical measurement and EDS analysis may be more accurate than the calculation from the XRD pattern or XPS spectrum. Therefore, the mole ratio of $Sb:Sb_2O_3$ in the Sb/Sb_2O_3 composite was estimated to be 9:1.

The electrochemical properties of the Sb/Sb_2O_3 composite were examined using a half-cell with Na metal as the counter electrode. Based on the half-cell reaction considered in this study, the sodiation of the composite is referred to as the discharging process, and the desodiation of the composite is referred to as the charging process.

Figure 4a shows the cycle performance and Coulombic efficiency of the Sb/Sb_2O_3 electrode at a current density of 66 mA g^{-1} over the voltage range of 0.01−2.50 V (vs Na^+/Na). The first discharge and charge capacities of the electrode were 772 mAh g^{-1} and 657 mAh g^{-1}, respectively, with a Coulombic efficiency of 85.2%. The charge capacity increased up to 670 mAh g^{-1} during the first three cycles, which may be attributed to the increase in the number of reaction sites and the reduction in the Na-ion diffusion length of the Sb/Sb_2O_3 composite with cycling. In the following cycles, the charge capacity faded slightly up to the 30th cycle, but the charge capacity was maintained at 615 mAh g^{-1} after 100 cycles, which corresponded to 91.84% of a maximum charge capacity (670 mAh g^{-1} in the third cycle). In particular, even at the high current density of 660 mA g^{-1}, the Sb/Sb_2O_3 electrode retained a 97.56% capacity retention during 100 cycles; the charge capacity of the Sb/Sb_2O_3 electrode was reduced from 549 mAh g^{-1} to 535 mAh g^{-1} (Figure S1). To the best of our knowledge, such a high specific capacity with excellent cycle stability has not yet been reported for Sb-based anode materials for use in Na-ion batteries.[5,6,11,13,16,19−21,28,30−36] Furthermore, this result is notable because the high capacity and stable cycle performance were achieved without using a binder, conductive agent, and any inactive matrix. Although the Coulombic efficiencies of the first few cycles were below 90%, the efficiency steadily increased to 96.97% by the 100th cycle. Low Coulombic efficiency is commonly attributed to irreversible capacity, which corresponds to consistent electrolyte decomposition on the surface of an electrode. In this study, the FEC was added to the electrolyte to form a stable and thin solid

DOI: 10.1021/acsami.5b04225
ACS Appl. Mater. Interfaces 2015, 7, 17264−17271

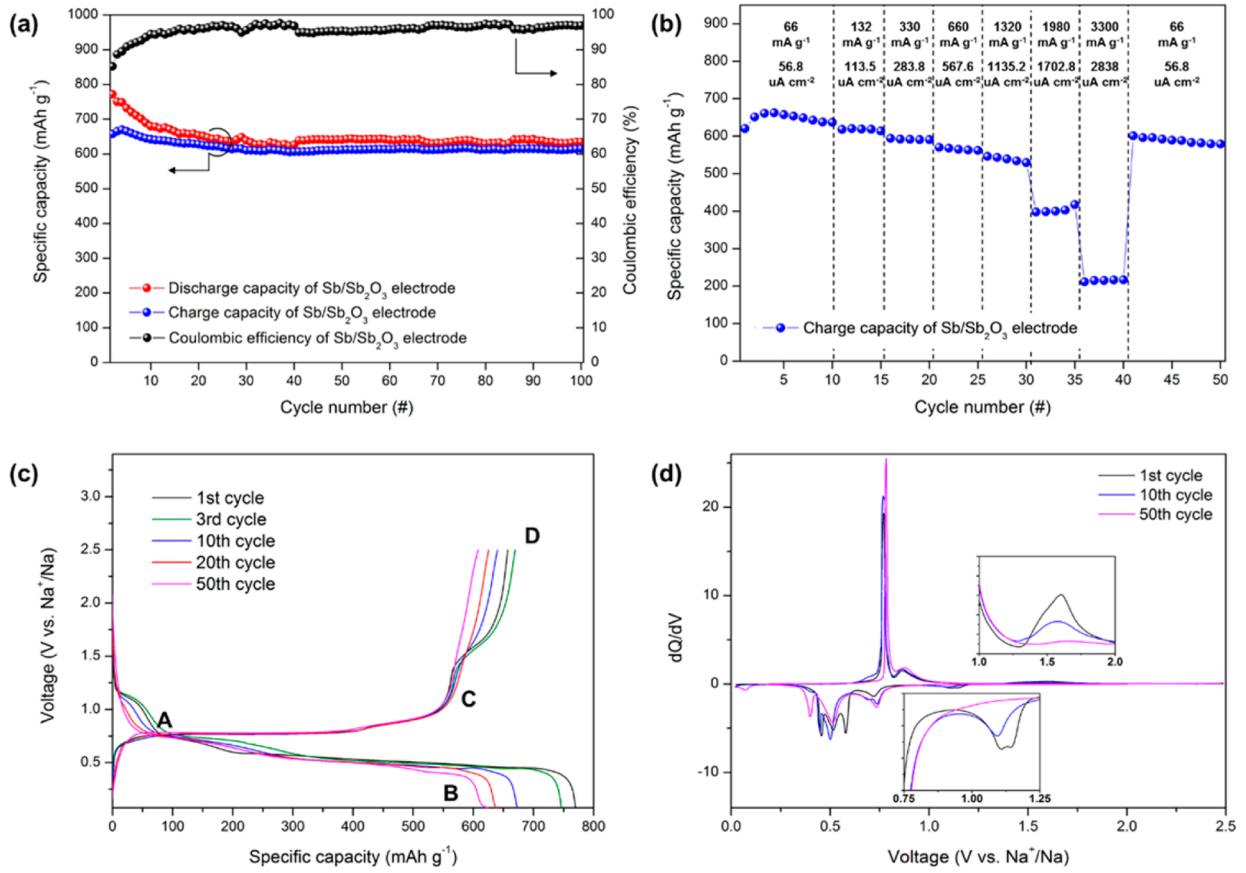

Figure 4. (a) Cycle performance and Coulombic efficiency of an Sb/Sb_2O_3 electrode at a constant current density of 66 mA g^{-1}, (b) rate capability of an Sb/Sb_2O_3 electrode at various current densities increasing from 66 to 3300 mA g^{-1} and returning to 66 mA g^{-1}, (c) charge–discharge voltage profiles of an Sb/Sb_2O_3 electrode at a constant current density of 66 mA g^{-1}, and (d) derivatives of charge–discharge voltage profiles for an Sb/Sb_2O_3 electrode at a constant current density of 66 mA g^{-1} over the potential range of 0.01–2.50 V (vs Na^+/Na).

electrolyte interphase (SEI) layer, which can promote a longer cycle life by modifying the surface passivation layer.[37] Another possible reason for the low Coulombic efficiency is that the reversibility of the conversion reaction between Na_2O and Sb_2O_3 is too low because this reaction is thermodynamically and kinetically unfavorable at room temperature.[19,21,22] Despite the irreversible capacity loss, it appears from the excellent cycle stability of the Sb/Sb_2O_3 electrode that most of the Sb/Sb_2O_3 composite reversibly reacted with Na and that the abrupt capacity degradation caused by the detachment of active materials was significantly suppressed (Figure S2).

Figure 4b shows the rate capability of the Sb/Sb_2O_3 electrode with the current density increased from 66 to 3300 mA g^{-1} and returned to 66 mA g^{-1}. The Sb/Sb_2O_3 electrode delivered specific charge capacities of 637, 619, 594, 571, 546, 398, and 212 mAh g^{-1} at current densities of 66, 132, 330, 660, 1320, 1980, and 3300 mA g^{-1}, respectively. When the current density was returned to 66 mA g^{-1}, the charge capacity recovered to 601 mAh g^{-1}. This result demonstrates that the Sb/Sb_2O_3 composite can endure high-rate cycling without structural damage. In particular, it is noteworthy that the rate performance of the Sb/Sb_2O_3 composite is comparable to that of other Sb oxide anode materials,[19−21,32,33] despite the absence of a conductive carbon or graphene composite. The superior rate capability is presumably due to inherently high electrical contact between the Sb/Sb_2O_3 composite and the nodule-type substrate owing to the use of the electrodeposition process.

Figure 4c displays the charge–discharge profiles for the Sb/Sb_2O_3 electrode at a rate of 66 mA g^{-1} between 0.01 and 2.50 V. The discharge curve shows three distinct plateaus located at 1.10, 0.74, and 0.55 V, and the charge curve shows three corresponding plateaus centered at 0.77, 0.87, and 1.60 V, which were clearly identified from the differential capacity plots shown in Figure 4d. According to previous studies on the alloying/dealloying reaction and conversion reaction of Sb-based electrodes[4,6,19,28,32,36,38] and Sn-based electrodes,[8,24,39−43] the reduction plateau at 1.10 V can be assigned to the reduction reaction of Sb_2O_3, and the plateaus at 0.74 and 0.55 V are due to the formation of intermediate Na_xSb and hexagonal Na_3Sb phases, respectively. In the following charge process, the oxidation plateaus at 0.77 and 0.87 V are related to the dealloying reactions of Na_3Sb. The charge plateau at 1.60 V corresponds to the oxidation reaction of Sb. Therefore, the plateaus at 1.10 and 1.60 V are expected to be the conversion reaction between Sb_2O_3 and Na_2O. Indeed, the charge–discharge profiles for a pure Sb electrode did not show a discharge plateau at 1.10 V and charge plateau at 1.60 V (Figure S3). This indicates that the conversion reaction between Sb_2O_3 and Na_2O occurred additionally to the alloying/dealloying reaction of Sb with Na.

Another notable feature of the charge–discharge curves obtained during cycling is that the capacity reduction of the Sb/Sb_2O_3 electrode was mainly resulted from the decreased capacity of the conversion reaction. As shown in Figure 4c, the capacity at 1.10/1.60 V (the conversion reaction between

DOI: 10.1021/acsami.5b04225
ACS Appl. Mater. Interfaces 2015, 7, 17264–17271

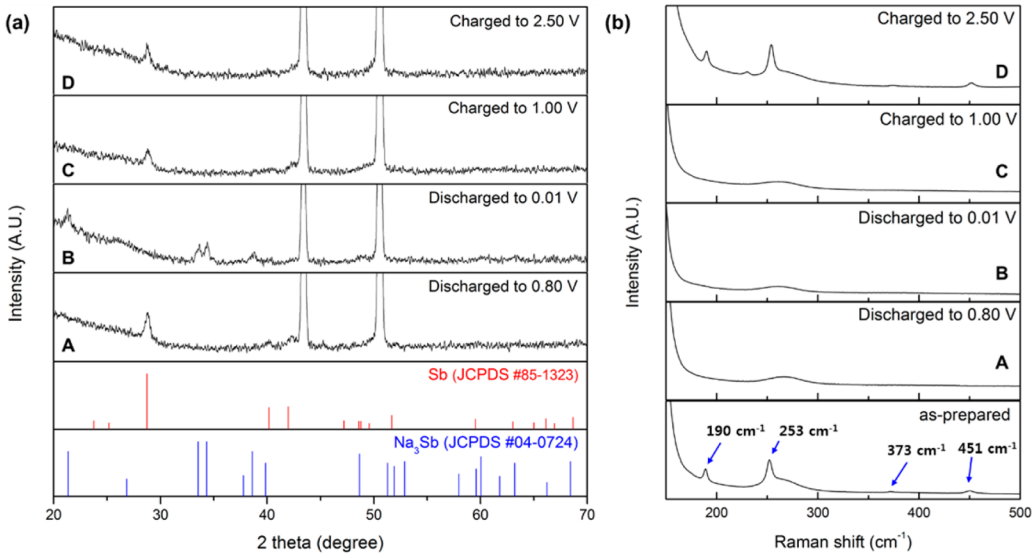

Figure 5. (a) XRD patterns and (b) Raman spectra of an Sb/Sb_2O_3 electrode when discharged and charged to selected potentials, as noted in Figure 4c (A: discharged to 0.80 V, B: discharged to 0.01 V, C: charged to 1.00 V, and D: charged to 2.50 V in the first cycle, respectively).

Sb_2O_3 and Na_2O) was approximately 90 mAh g^{-1} in the first and third cycles, but this contribution gradually decreased to 35 mAh g^{-1} during 100 cycles. On the other hand, the charge capacity of the alloying/dealloying reaction remained nearly unchanged at approximately 580 mAh g^{-1} over 100 cycles. This finding reveals that the capacity fading observed during the first 20 cycles was entirely caused by the deterioration in the reversibility of the conversion reaction, which is well in accordance with the SnO_2 electrodes.[39−43] In addition, the alloying/dealloying reaction of Sb with Na is completely reversible, whereas the conversion reaction of Sb_2O_3 appears to be partially reversible.

To better understand the reaction mechanism of the Sb/Sb_2O_3 composite, *ex situ* analyses were performed on the Sb/Sb_2O_3 electrodes that had been discharged at A (0.80 V) and B (0.01 V) or charged at C (1.00 V) and D (2.50 V), as noted in Figure 4c. Figure 5a shows that the phase transition of the composite during cycling was identified by *ex situ* XRD analysis. The broad peak in the range of 20−30° observed in all samples was due to the Kapton tape, which was used to prevent contact between the electrode and air/moisture. At the end of the first discharge plateau (A), the diffraction peaks of Sb_2O_3 completely disappeared, and only the rhombohedral Sb peaks were observed, confirming that Sb_2O_3 had been converted to metallic Sb and Na_2O by the conversion reaction. Although the diffraction peaks of Sb_2O_3 vanished, the peak associated with Na_2O, the reaction product to be formed from the conversion reaction, was not observed at 0.80 V. This finding is attributed to the fact that verifying the presence of Na_2O using XRD analysis is difficult due to the amorphous or nanocrystalline nature of Na_2O.[20,22] At full sodiation to 0.01 V, new peaks at 21.3, 33.6, and 34.4° appeared, which were indexed to the (101), (110), and (103) planes of hexagonal Na_3Sb. This behavior is quite similar to that of the typical metal Sb alloying reaction[4,6,36,38] but differs from that observed for an Sb_2O_3 electrode by Hu et al.[20] In the following charge process, at 1.00 V during charging (C), the hexagonal Na_3Sb phase disappeared and the rhombohedral Sb phase reappeared, which demonstrated that Na_3Sb was completely converted to Sb by Na extraction. In addition, at full desodiation at 2.50 V, the diffraction peaks of Sb were maintained without a change in the XRD patterns.

It is difficult to confirm the phase formed by the conversion reaction using *ex situ* XRD analysis, and hence we employed *ex situ* Raman spectroscopy to examine the samples. According to Raman spectroscopic studies,[44−46] the Raman spectrum of cubic Sb_2O_3 over the range of 150−500 cm^{-1} has four distinct peaks at 190, 253, 373, and 451 cm^{-1}. The intense narrow bands at 451 and 253 cm^{-1} (A_1) were responsible for the symmetric combination of $\nu_{sym}(SbO_3)$ and $\nu_{sym}(Sb{\rightarrow}O{\leftarrow}Sb)$ and for the symmetric combination of $\delta_{sym}(SbO_3)$ and $\delta_{sym}(Sb{\rightarrow}O{\leftarrow}Sb)$, respectively. The weak bands were observed at 373 and 190 cm^{-1} (T_2), which corresponded to the asymmetric combination of $\nu_{sym}(SbO_3)$ and $\nu_{sym}(Sb{\rightarrow}O{\leftarrow}Sb)$ and to the asymmetric combination of $\delta_{asym}(SbO_3)$ and $\delta_{sym}(Sb{\rightarrow}O{\leftarrow}Sb)$, respectively. As shown in Figure 5b, the Raman peaks of the as-prepared Sb/Sb_2O_3 composite were identical to those of cubic Sb_2O_3.[44−46] The Raman peaks associated with cubic Sb_2O_3 were not obtained in the discharged states (A, B) or in the charged state at 1.00 V (C), but the peaks were observed in the charged state at 2.50 V (D). These results indicate that the Sb_2O_3 phase was formed again by the reverse conversion reaction ($2Sb + 3Na_2O \rightarrow Sb_2O_3 + 6Na^+ + 6e^-$) when the electrode was charged to 2.50 V. Based on the results described above, the sodiation/desodiation mechanism of the Sb/Sb_2O_3 composite is proposed as depicted in Table 1.

The x value or the mole ratio of Sb_2O_3 to Sb for the Sb/Sb_2O_3 composite was estimated to be 0.1 in this work, and hence the theoretical capacities of the alloying/dealloying reaction (reaction 8, 9, 10) and conversion reaction (reaction 7, 11) were calculated to be approximately 637 and 115 mAh g^{-1}, respectively. Therefore, the total theoretical capacity of the Sb/Sb_2O_3 electrode was expected to be 752 mAh g^{-1} that is higher than the theoretical capacity of Sb (660 mAh g^{-1}). In this respect, the charge capacity of 670 mAh g^{-1} at the third cycle represents approximately 89% utilization of the theoretical value of 752 mAh g^{-1}.

DOI: 10.1021/acsami.5b04225
ACS Appl. Mater. Interfaces 2015, 7, 17264−17271

Table 1. Sodiation/Desodiation Reactions of Sb/Sb_2O_3 Composites

process	voltage	reaction	no.
Discharge (Sodiation)	~0.80 V	$Sb + xSb_2O_3 + 6xNa^+ + 6xe^- \rightarrow (2x + 1)Sb + 3xNa_2O$	(7)
	~0.58 V	$(2x + 1)Sb + 3xNa_2O + y(2x + 1)Na^+ + y(2x + 1)e^- \rightarrow (2x + 1)Na_ySb + 3xNa_2O$	(8)
	~0.01 V	$(2x + 1)Na_ySb + 3xNa_2O + (3 - y)(2x + 1)Na^+ + (3 - y)(2x + 1)e^- \rightarrow (2x + 1)Na_3Sb + 3xNa_2O$	(9)
Charge (Desodiation)	~1.00 V	$(2x + 1)Na_3Sb + 3xNa_2O \rightarrow (2x + 1)Sb + 3xNa_2O + (6x + 3)Na^+ + (6x + 3)e^-$	(10)
	~2.50 V	$(2x + 1)\ Sb + 3xNa_2O \rightarrow Sb + xSb_2O_3 + 6xNa^+ + 6xe^-$	(11)

4. CONCLUSIONS

Sb/Sb_2O_3 composites were successfully synthesized by a one-step electrodeposition process, and its electrochemical properties and reaction mechanism as an electrode material for Na-ion batteries were investigated. The Sb/Sb_2O_3 composites were composed of approximately 90 mol % metallic Sb and 10 mol % crystalline Sb_2O_3. Because the composite utilizes not only the alloying/dealloying reaction of Sb ($Sb + 3Na^+ + 3e^- \leftrightarrow Na_3Sb$) but also the conversion reaction between Na_2O and Sb_2O_3 ($Sb_2O_3 + 6Na^+ + 6e^- \leftrightarrow 2Sb + 3Na_2O$), the electrode exhibited a higher charge capacity of 670 mAh g^{-1} than the theoretical capacity of Sb (660 mAh g^{-1}). Although the reversibility of the conversion reaction was deteriorated with cycling, this partially reversible conversion reaction not only offers an additional specific capacity of approximately 35 mAh g^{-1} but also generates amorphous Na_2O, which can act as an effective buffer against volume changes during the alloying/dealloying of Sb. As a consequence, the Sb/Sb_2O_3 composite showed excellent cycle performance with the higher charge capacities compared with the previous Sb-based electrodes. Although further research is required to improve the cyclability and rate capability, the results demonstrate the possibility of producing a high-capacity Sb/Sb_2O_3 anode material for use in rechargeable Na-ion batteries.

■ ASSOCIATED CONTENT

Supporting Information

Cycle performance of an Sb/Sb_2O_3 electrode at a high current density of 660 mA g^{-1}, SEM images on the surface of the Sb/Sb_2O_3 electrode after 100 cycles, and charge−discharge profiles and cycle performance of Sb powder and Sb/Sb_2O_3 composites at a constant current density of 66 mA g^{-1}. The Supporting Information is available free of charge on the ACS Publications website at DOI: 10.1021/acsami.5b04225.

■ AUTHOR INFORMATION

Corresponding Authors

*(D.H.N.) E-mail: dhnam@kaist.ac.kr, Phone: +82-42-350-5326.

*(H.K.) E-mail: hskwon@kaist.ac.kr. Phone: +82-42-350-3326.

Notes

The authors declare no competing financial interest.

■ ACKNOWLEDGMENTS

This work was supported by the Center for Inorganic Photovoltaic Materials (no. 2013-001796) through a grant funded by the Korea Government (Ministry of Science, ICT and Future Planning). This work was also funded by POONGSAN.

■ REFERENCES

(1) Kim, S.-W.; Seo, D.-H.; Ma, X.; Ceder, G.; Kang, K. Electrode Materials for Rechargeable Sodium-Ion Batteries: Potential Alternatives to Current Lithium-Ion Batteries. *Adv. Energy Mater.* **2012**, *2*, 710−721.

(2) Slater, M. D.; Kim, D.; Lee, E.; Johnson, C. S. Sodium-Ion Batteries. *Adv. Funct. Mater.* **2013**, *23*, 947−958.

(3) Dahbi, M.; Yabuuchi, N.; Kubota, K.; Tokiwa, K.; Komaba, S. Negative Electrodes for Na-Ion Batteries. *Phys. Chem. Chem. Phys.* **2014**, *16*, 15007−15028.

(4) Darwiche, A.; Marino, C.; Sougrati, M. T.; Fraisse, B.; Stievano, L.; Monconduit, L. Better Cycling Performances of Bulk Sb in Na-Ion Batteries Compared to Li-Ion Systems: An Unexpected Electrochemical Mechanism. *J. Am. Chem. Soc.* **2012**, *134*, 20805−20811.

(5) Zhu, Y.; Han, X.; Xu, Y.; Liu, Y.; Zheng, S.; Xu, K.; Hu, L.; Wang, C. Electrospun Sb/C Fibers for a Stable and Fast Sodium-Ion Battery Anode. *ACS Nano* **2013**, *7*, 6378−6386.

(6) Nam, D.-H.; Hong, K.-S.; Lim, S.-J.; Kwon, H.-S. Electrochemical Synthesis of a Three-Dimensional Porous Sb/Cu_2Sb Anode for Na-Ion Batteries. *J. Power Sources* **2014**, *247*, 423−427.

(7) Zhu, H.; Jia, Z.; Chen, Y.; Weadock, N.; Wan, J.; Vaaland, O.; Han, X.; Li, T.; Hu, L. Tin Anode for Sodium-Ion Batteries Using Natural Wood Fiber as a Mechanical Buffer and Electrolyte Reservoir. *Nano Lett.* **2013**, *13*, 3093−3100.

(8) Nam, D.-H.; Kim, T.-H.; Hong, K.-S.; Kwon, H.-S. Template-Free Electrochemical Synthesis of Sn Nanofibers as High-Performance Anode Materials for Na-Ion Batteries. *ACS Nano* **2014**, *8*, 11824−11835.

(9) Farbod, B.; Cui, K.; Kalisvaart, W. P.; Kupsta, M.; Zahiri, B.; Kohandehghan, A.; Lotfabad, E. M.; Li, Z.; Luber, E. J.; Mitlin, D. Anodes for Sodium Ion Batteries Based on Tin−Germanium−Antimony Alloys. *ACS Nano* **2014**, *8*, 4415−4429.

(10) Abel, P. R.; Lin, Y.-M.; de Souza, T.; Chou, C.-Y.; Gupta, A.; Goodenough, J. B.; Hwang, G. S.; Heller, A.; Mullins, C. B. Nanocolumnar Germanium Thin Films as a High-Rate Sodium-Ion Battery Anode Material. *J. Phys. Chem. C* **2013**, *117*, 18885−18890.

(11) Baggetto, L.; Marszewski, M.; Górka, J.; Jaroniec, M.; Veith, G. M. AlSb Thin Films as Negative Electrodes for Li-Ion and Na-Ion Batteries. *J. Power Sources* **2013**, *243*, 699−705.

(12) Darwiche, A.; Toiron, M.; Sougrati, M. T.; Fraisse, B.; Stievano, L.; Monconduit, L. Performance and Mechanism of $FeSb_2$ as Negative Electrode for Na-Ion Batteries. *J. Power Sources* **2015**, *280*, 588−592.

(13) Baggetto, L.; Allcorn, E.; Unocic, R. R.; Manthiram, A.; Veith, G. M. Mo_3Sb_7 as a Very Fast Anode Material for Lithium-Ion and Sodium-Ion Batteries. *J. Mater. Chem. A* **2013**, *1*, 11163−11169.

(14) Wu, L.; Pei, F.; Mao, R.; Wu, F.; Wu, Y.; Qian, J.; Cao, Y.; Ai, X.; Yang, H. SiC−Sb−C Nanocomposites as High-Capacity and Cycling-

DOI: 10.1021/acsami.5b04225
ACS Appl. Mater. Interfaces 2015, 7, 17264−17271

Stable Anode for Sodium-Ion Batteries. *Electrochim. Acta* **2013**, *87*, 41−45.
(15) Zhou, X.; Dai, Z.; Bao, J.; Guo, Y.-G. Wet Milled Synthesis of an Sb/MWCNT Nanocomposite for Improved Sodium Storage. *J. Mater. Chem. A* **2013**, *1*, 13727−13731.
(16) Zhou, X.; Zhong, Y.; Yang, M.; Hu, M.; Wei, J.; Zhou, Z. Sb Nanoparticles Decorated N-Rich Carbon Nanosheets as Anode Materials for Sodium Ion Batteries with Superior Rate Capability and Long Cycling Stability. *Chem. Commun.* **2014**, *50*, 12888−12891.
(17) Valvo, M.; Lindgren, F.; Lafont, U.; Björefors, F.; Edström, K. Towards More Sustainable Negative Electrodes in Na-Ion Batteries Via Nanostructured Iron Oxide. *J. Power Sources* **2014**, *245*, 967−978.
(18) Wu, L.; Hu, X.; Qian, J.; Pei, F.; Wu, F.; Mao, R.; Ai, X.; Yang, H.; Cao, Y. A Sn-SnS-C Nanocomposite as Anode Host Materials for Na-Ion Batteries. *J. Mater. Chem. A* **2013**, *1*, 7181−7184.
(19) Sun, Q.; Ren, Q.-Q.; Li, H.; Fu, Z.-W. High Capacity Sb_2O_4 Thin Film Electrodes for Rechargeable Sodium Battery. *Electrochem. Commun.* **2011**, *13*, 1462−1464.
(20) Hu, M.; Jiang, Y.; Sun, W.; Wang, H.; Jin, C.; Yan, M. Reversible Conversion-Alloying of Sb_2O_3 as a High-Capacity, High-Rate, and Durable Anode for Sodium Ion Batteries. *ACS Appl. Mater. Interfaces* **2014**, *6*, 19449−19455.
(21) Li, K.; Liu, H.; Wang, G. Sb_2O_3 Nanowires as Anode Material for Sodium-Ion Battery. *Arabian J. Sci. Eng.* **2014**, *39*, 6589−6593.
(22) Klein, F.; Jache, B.; Bhide, A.; Adelhelm, P. Conversion Reactions for Sodium-Ion Batteries. *Phys. Chem. Chem. Phys.* **2013**, *15*, 15876−15887.
(23) Bryngelsson, H.; Eskhult, J.; Nyholm, L.; Herranen, M.; Alm, O.; Edström, K. Electrodeposited Sb and Sb/Sb_2O_3 Nanoparticle Coatings as Anode Materials for Li-Ion Batteries. *Chem. Mater.* **2007**, *19*, 1170−1180.
(24) Nam, D.-H.; Hong, K.-S.; Lim, S.-J.; Kim, T.-H.; Kwon, H.-S. Electrochemical Properties of Electrodeposited Sn Anodes for Na-Ion Batteries. *J. Phys. Chem. C* **2014**, *118*, 20086−20093.
(25) Nam, D.-H.; Kim, M.-J.; Lim, S.-J.; Song, I.-S.; Kwon, H.-S. Single-Step Synthesis of Polypyrrole Nanowires by Cathodic Electropolymerization. *J. Mater. Chem. A* **2013**, *1*, 8061−8068.
(26) Dixit, V. K.; Keerthi, K. S.; Bhat, H. L.; Bera, P.; Hegde, M. S. Structural and Compositional Analysis of $InBi_xAs_ySb_{(1-x-y)}$ Films Grown on GaAs(0 0 1) Substrates by Liquid Phase Epitaxy. *Appl. Surf. Sci.* **2003**, *220*, 321−326.
(27) Li, L.; Zhang, Y. X.; Fang, X. S.; Zhai, T. Y.; Liao, M. Y.; Wang, H. Q.; Li, G. H.; Koide, Y.; Bando, Y.; Golberg, D. Sb_2O_3 Nanobelt Networks for Excellent Visible-Light-Range Photodetectors. *Nanotechnology* **2011**, *22*, 165704.
(28) Zhou, X.; Liu, X.; Xu, Y.; Liu, Y.; Dai, Z.; Bao, J. An SbO_x/Reduced Graphene Oxide Composite as a High-Rate Anode Material for Sodium-Ion Batteries. *J. Phys. Chem. C* **2014**, *118*, 23527−23534.
(29) McIntyre, N. S.; Stanchell, F. W. Preferential Sputtering in Oxides as Metals and Revealed by X-Ray Photoelectron Spectroscopy. *J. Vac. Sci. Technol.* **1979**, *16*, 798−802.
(30) Qian, J.; Chen, Y.; Wu, L.; Cao, Y.; Ai, X.; Yang, H. High Capacity Na-Storage and Superior Cyclability of Nanocomposite Sb/C Anode for Na-Ion Batteries. *Chem. Commun.* **2012**, *48*, 7070−7072.
(31) Wu, L.; Hu, X.; Qian, J.; Pei, F.; Wu, F.; Mao, R.; Ai, X.; Yang, H.; Cao, Y. Sb-C Nanofibers with Long Cycle Life as an Anode Material for High-Performance Sodium-Ion Batteries. *Energy Environ. Sci.* **2014**, *7*, 323−328.
(32) Li, N.; Liao, S.; Sun, Y.; Song, H. W.; Wang, C. X. Uniformly Dispersed Self-Assembled Growth of Sb_2O_3/Sb@Graphene Nanocomposites on a 3D Carbon Sheet Network for High Na-Storage Capacity and Excellent Stability. *J. Mater. Chem. A* **2015**, *3*, 5820−5828.
(33) Nam, D.-H.; Hong, K.-S.; Lim, S.-J.; Kim, M.-J.; Kwon, H.-S. High-Performance Sb/Sb_2O_3 Anode Materials Using a Polypyrrole Nanowire Network for Na-Ion Batteries. *Small* **2015**, *11*, 2885−2892.
(34) Xiao, L.; Cao, Y.; Xiao, J.; Wang, W.; Kovarik, L.; Nie, Z.; Liu, J. High Capacity, Reversible Alloying Reactions in SnSb/C Nanocomposites for Na-Ion Battery Applications. *Chem. Commun.* **2012**, *48*, 3321−3323.
(35) Darwiche, A.; Sougrati, M. T.; Fraisse, B.; Stievano, L.; Monconduit, L. Facile Synthesis and Long Cycle Life of SnSb as Negative Electrode Material for Na-Ion Batteries. *Electrochem. Commun.* **2013**, *32*, 18−21.
(36) Baggetto, L.; Hah, H.-Y.; Jumas, J.-C.; Johnson, C. E.; Johnson, J. A.; Keum, J. K.; Bridges, C. A.; Veith, G. M. The Reaction Mechanism of SnSb and Sb Thin Film Anodes for Na-Ion Batteries Studied by X-Ray Diffraction, 119Sn and 121Sb Mössbauer Spectroscopies. *J. Power Sources* **2014**, *267*, 329−336.
(37) Komaba, S.; Ishikawa, T.; Yabuuchi, N.; Murata, W.; Ito, A.; Ohsawa, Y. Fluorinated Ethylene Carbonate as Electrolyte Additive for Rechargeable Na Batteries. *ACS Appl. Mater. Interfaces* **2011**, *3*, 4165−4168.
(38) Baggetto, L.; Ganesh, P.; Sun, C.-N.; Meisner, R. A.; Zawodzinski, T. A.; Veith, G. M. Intrinsic Thermodynamic and Kinetic Properties of Sb Electrodes for Li-Ion and Na-Ion Batteries: Experiment and Theory. *J. Mater. Chem. A* **2013**, *1*, 7985−7994.
(39) Su, D.; Ahn, H.-J.; Wang, G. SnO_2@Graphene Nanocomposites as Anode Materials for Na-Ion Batteries with Superior Electrochemical Performance. *Chem. Commun.* **2013**, *49*, 3131−3133.
(40) Wang, Y.; Su, D.; Wang, C.; Wang, G. SnO_2@MWCNT Nanocomposite as a High Capacity Anode Material for Sodium-Ion Batteries. *Electrochem. Commun.* **2013**, *29*, 8−11.
(41) Gu, M.; Kushima, A.; Shao, Y.; Zhang, J.-G.; Liu, J.; Browning, N. D.; Li, J.; Wang, C. Probing the Failure Mechanism of SnO_2 Nanowires for Sodium-Ion Batteries. *Nano Lett.* **2013**, *13*, 5203−5211.
(42) Wang, Y.-X.; Lim, Y.-G.; Park, M.-S.; Chou, S.-L.; Kim, J. H.; Liu, H.-K.; Dou, S.-X.; Kim, Y.-J. Ultrafine SnO_2 Nanoparticle Loading onto Reduced Graphene Oxide as Anodes for Sodium-Ion Batteries with Superior Rate and Cycling Performances. *J. Mater. Chem. A* **2014**, *2*, 529−534.
(43) Górka, J.; Baggetto, L.; Keum, J. K.; Mahurin, S. M.; Mayes, R. T.; Dai, S.; Veith, G. M. The Electrochemical Reactions of SnO_2 with Li and Na: A Study Using Thin Films and Mesoporous Carbons. *J. Power Sources* **2015**, *284*, 1−9.
(44) Mestl, G.; Ruiz, P.; Delmon, B.; Knozinger, H. Sb_2O_3/Sb_2O_4 in Reducing/Oxidizing Environments: An in Situ Raman Spectroscopy Study. *J. Phys. Chem.* **1994**, *98*, 11276−11282.
(45) Gilliam, S. J.; Jensen, J. O.; Banerjee, A.; Zeroka, D.; Kirkby, S. J.; Merrow, C. N. A Theoretical and Experimental Study of Sb_4O_6: Vibrational Analysis, Infrared, and Raman Spectra. *Spectrochim. Acta, Part A* **2004**, *60*, 425−434.
(46) Voit, E. I.; Panasenko, A. E.; Zemnukhova, L. A. Vibrational Spectroscopic and Quantum Chemical Study of Antimony(III) Oxide. *J. Struct. Chem.* **2009**, *50*, 60−66.

DOI: 10.1021/acsami.5b04225
ACS Appl. Mater. Interfaces 2015, 7, 17264−17271